MIKE 21 Wave Model FM

Hydrodynamic module

Validation Report

DHI A/S headquarters
Agern Allé 5
DK-2970 Hørsholm
Denmark

+45 4516 9200 Telephone
mike@dhigroup.com
www.mikepoweredbydhi.com

Company Registration No.: DK36466871

CONTENTS

MIKE 21 Wave Model FM
Hydrodynamic Module
Validation Report

1 Vision and scope

MIKE 21 Wave Model FM is a phase-resolving wave model formulated in the time domain. The governing equations are the 2D Boussinesq-type equations of Madsen and Sørensen (1992). These equations provide excellent accuracy in shoaling as well as in linear dispersion for the ratio of the water depth to the deep water wave length, h/L_0, as large as 0.5. The deep water wave length is defined as $L_0=gT^2/(2\pi)$, where T is the wave period and g is the gravity. The numerical techniques applied are based on an unstructured (flexible) mesh approach. The spatial discretization is performed using a cell-centered finite volume method with a shock-capturing scheme where the interface fluxes are calculated using an approximate Riemann solver. A set of well-defined test cases are used for the validation of the model.

For comparison, simulations have also been performed using MIKE 21 Boussinesq Model and MIKE 3 Wave Model FM. Both models are also phase-resolving wave models formulated in the time domain. MIKE 21 Boussinesq Model is also solving the 2D Boussinesq-type equations of Madsen and Sørensen (1992), but the spatial discretization is based on the finite difference approach on a structured grid. MIKE 3 Wave model FM is solving the fully nonlinear Navier-Stokes equations with the free surface described by a height function. The basic numerical approach used for this model is the same as for MIKE 21 Wave Model FM.

2 Methodology

2.1 Hardware

The validation tests have been performed using the following hardware platform:

Table 2.1 Hardware platform used for validation

Computer	Processor	Memory	Operating system	GPUs
DELL Precision 7920 Rack	2 x Intel®Xeon® Gold 6136 (12 cores, 3.00 GHz)	64 GB	Windows 10 Enterprise, 64-bit	2 x NVIDIA RTX A6000

2.2 Software

All validation tests have been performed using the Release 2025 version of the MIKE by DHI software.

3 Validation Test Cases

3.1 Propagation of Regular waves over a Submerged Bar

3.1.1 Description

Wave transformation over a submerged bar is a very demanding test case for most wave models as it involves non-linear shoaling and growth of bound harmonics on the uphill slope and subsequent release of higher harmonics on the downhill slope. After the bar, these harmonics will propagate as free waves. Luth et al. (1994) performed a series of accurate flume experiments for wave transformation over a trapezoidal bar with an upward slope of 1/20, a downward slope of 1/40, a constant depth of 0.4m before and after the bar and a depth of 0.1m on top of the bar (see Figure 3.1). As an example from the test series is selected the case for regular nonbreaking waves with wave period 2.02s and wave height 0.02m.

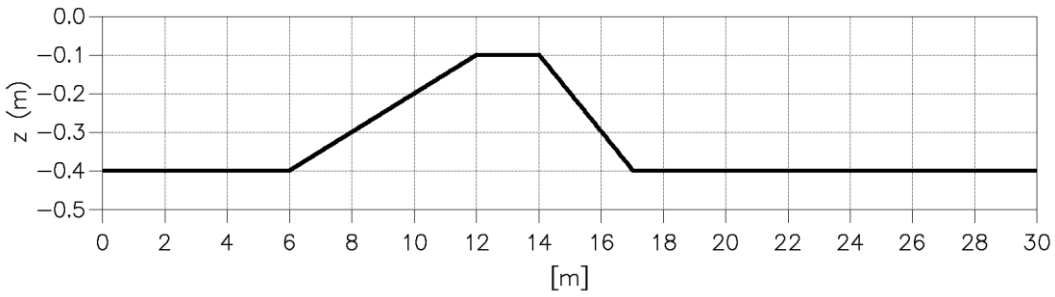

Figure 3.1 Bed profile.

3.1.2 Setup

This test case is a one-dimensional flow problem. Hence, a one-element wide channel is used in the simulation. The mesh consists of quadrilateral elements with an edge length of 0.02m. The incoming waves are specified using a relaxation zone: Line from (x,y)=(2.0m, 0.05m) to (x,y)=(2.0m, 0.0m) and the width of the ramp-up zone is 1.8m. The waves are generated using 3rd order Boussinesq theory. The outgoing waves at the downstream boundary are absorbed using a 4m wide sponge layer. Simulations have been performed without the Riemann solver. No eddy viscosity has been applied.

3.1.3 Results

In Figure 3.2-Figure 3.5 the measured and calculated time series of surface elevations at x=13.5m, x=17.3m, x=19.0m and x=21.0m are shown. Figure 3.6 shows the amplitude for the measured and the computed higher harmonics along the channel. For comparison the results using the MIKE 21 Boussinesq Model are also shown in the figures. It is seen that the results using the MIKE 21 Wave Model FM and the MIKE 21 Boussinesq Model are almost identical. This is also expected because the two models are solving the same governing equations.

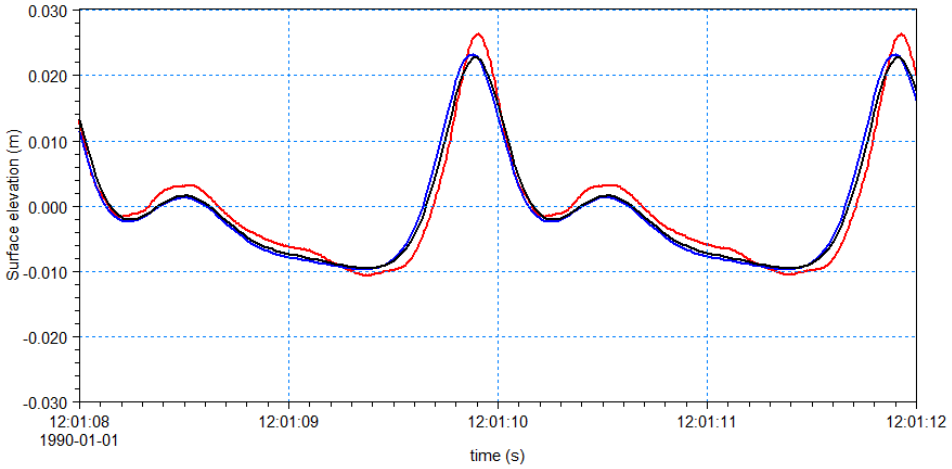

Figure 3.2 Computed and measured surface elevation at x=13.5m. Black line: MIKE 21 Wave Model FM; Blue line: MIKE 21 Boussinesq Model; Red line: Experimental data.

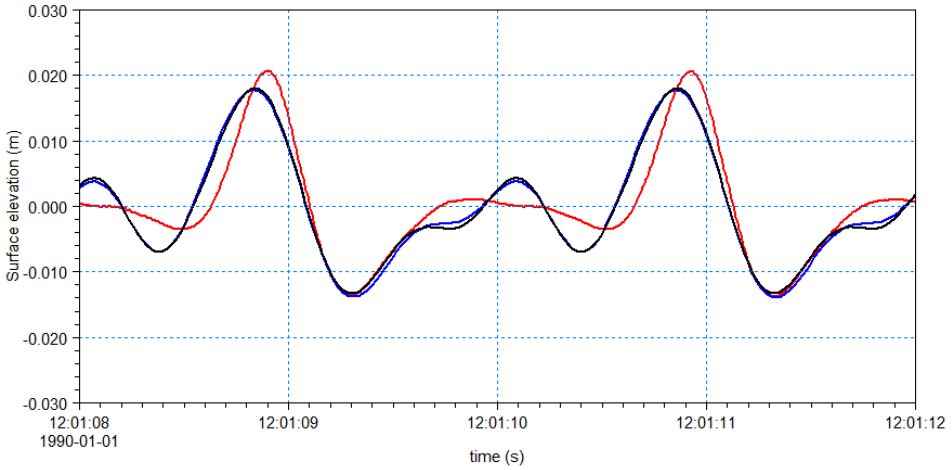

Figure 3.3 Computed and measured surface elevation at x=17.3m. Black line: MIKE 21 Wave Model FM; Blue line: MIKE 21 Boussinesq Model; Red line: Experimental data.

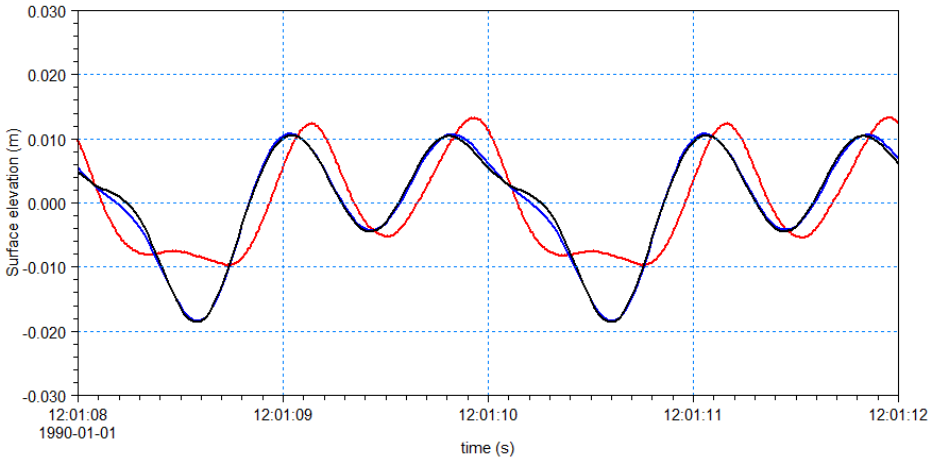

Figure 3.4 Computed and measured surface elevation at x=19.0m. Black line: MIKE 21 Wave Model FM; Blue line: MIKE 21 Boussinesq Model; Red line: Experimental data.

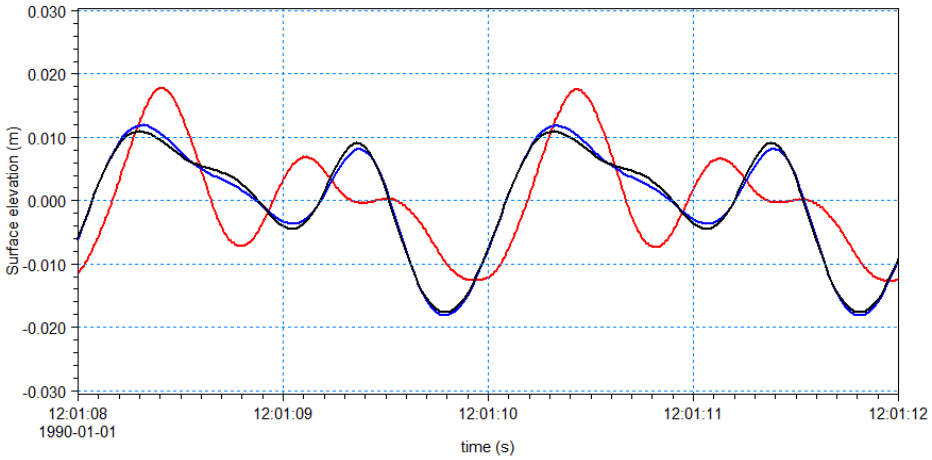

Figure 3.5 Computed and measured surface elevation at x=21.0m. Black line: MIKE 21 Wave Model FM; Blue line: MIKE 21 Boussinesq Model; Red line: Experimental data.

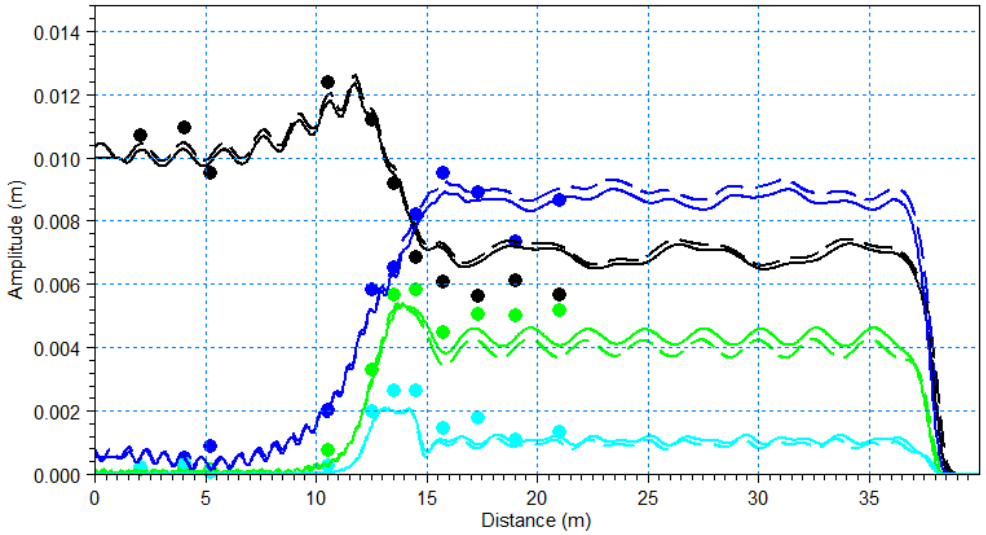

Figure 3.6 Wave amplitude for the higher harmonic along the channel. Black: First harmonic; Blue: Second harmonic.; Green: Third harmonic; Light blue: Forth harmonic; Solid line: MIKE 21 Wave Model, Dash line: MIKE 21 Boussinesq Wave Model, Circles: Experimental data.

3.2 Non-linear Refraction-Diffraction of Regular Waves over a Semicircular Shoal

3.2.1 Description

This test case is the non-linear refraction-diffraction of regular waves over a semicircular shoal. The problem was studied experimentally by Whalin (1971). For a presentation of numerical results, see e.g. Madsen and Sørensen (1992) and the references herein. The model area covers 6.096m x 36.576m with a depth variation given by

$$h(x,y)=\begin{cases}0.4572 & 0\le x\le 10.67-G\\ 0.4572+\frac{1}{25}(10.67-G-x) & 10.67-G\le x\le 18.29-G\\ 0.1524 & 18.29-G\le x\le 36.576\end{cases}$$

where

$$G(y)=\left[y(6.096-y)\right]^{1/2} \qquad 0\le y\le 6.096)$$

Whalin performed a series of experiments with different wave conditions. Here, calculations are performed for the case with a wave period of 2s and a wave amplitude of 0.0075m.

3.2.2 Setup

Both a structured and an unstructured mesh are used. The length of the domain is extended with 1.524m to account for the relaxation zone. The structured mesh consists of uniform quadrilateral elements with an edge length of 0.0508m, resulting in 90120 elements. The unstructured mesh consists of 89953 triangular elements. The incoming waves are specified using a relaxation zone: Line from (x,y)=(0.0m, 6.1m) to (x,y)=(0.0m, 0.0m) and the width of the ramp-up zone is 1m. The waves are generated using Boussinesq 3rd order wave theory. The outgoing waves at the downstream boundary are absorbed using a 6m wide sponge layer. A number of simulations have also been performed for different structured mesh resolutions. The edge lengths were 0.2032m, 0.1016m, 0.0508m and 0.0254m.

The simulations using structured mesh are performed without Riemann solver. For the simulations with unstructured mesh the HLLC solver is used with a Riemann factor of 0.05. No eddy viscosity has been applied.

3.2.3 Results

The incoming waves are linear, but after the focusing on the shoal, higher harmonics become significant due to non-linear effects. The focusing of the waves can be seen in Figure 3.7 showing an instantaneous surface elevation field calculated using the structured mesh. In Figure 3.8 the surface elevation along the centreline is shown using the two meshes. The energy transfer to higher harmonics is illustrated in Figure 3.9. Based on a Fourier analysis of the time series of the surface elevation at each grid point along the centreline, the spatial evolution of the first, second and third harmonics from the numerical simulations is compared with the experimental data. The results using the structured and the unstructured mesh are almost identical and the agreement with the measurements is quite good. A similar Fourier analysis is shown in Figure 3.10 for different structured mesh resolutions.

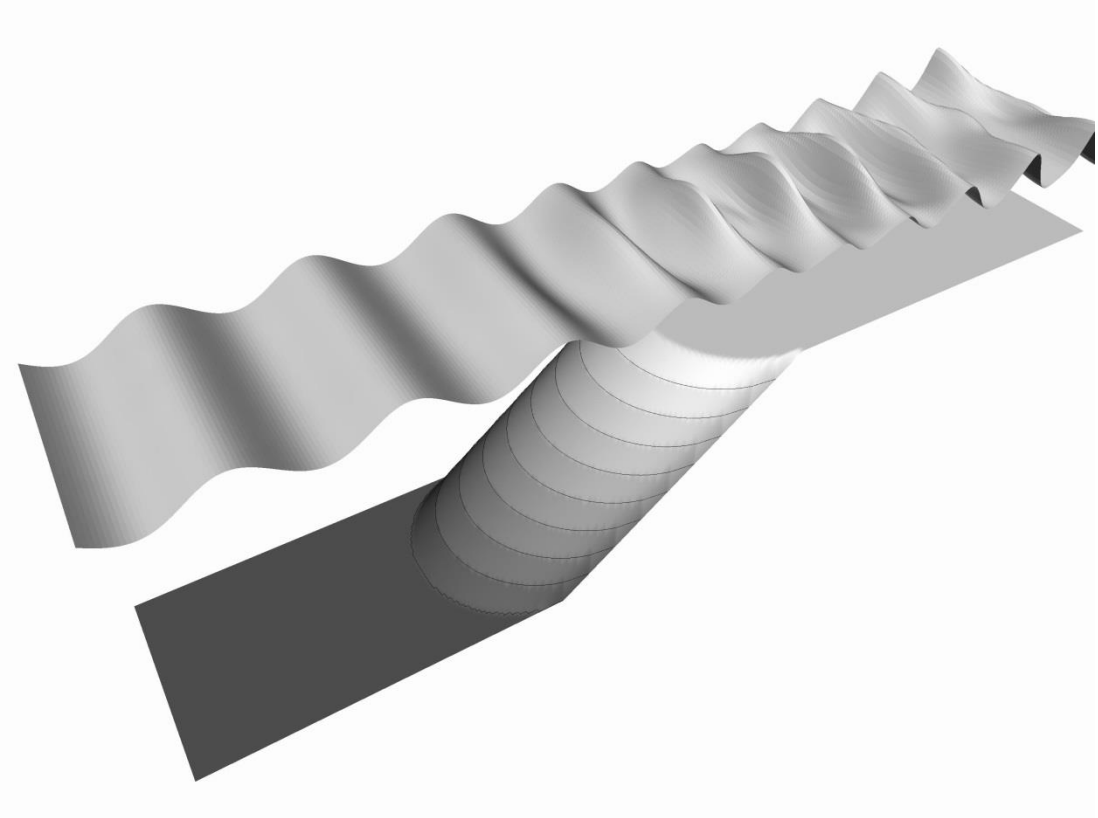

Figure 3.7 Instantaneous surface elevation calculated using structured mesh shown over the bathymetry.

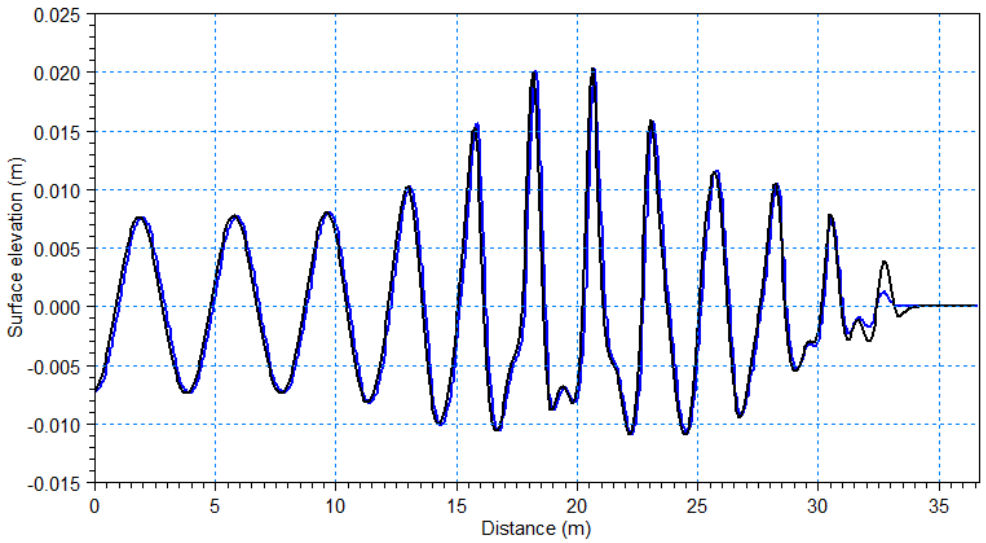

Figure 3.8 Surface elevation along the centreline (T = 2s and H = 0.015m). Black line: structured mesh; Blue line: Unstructured mesh.

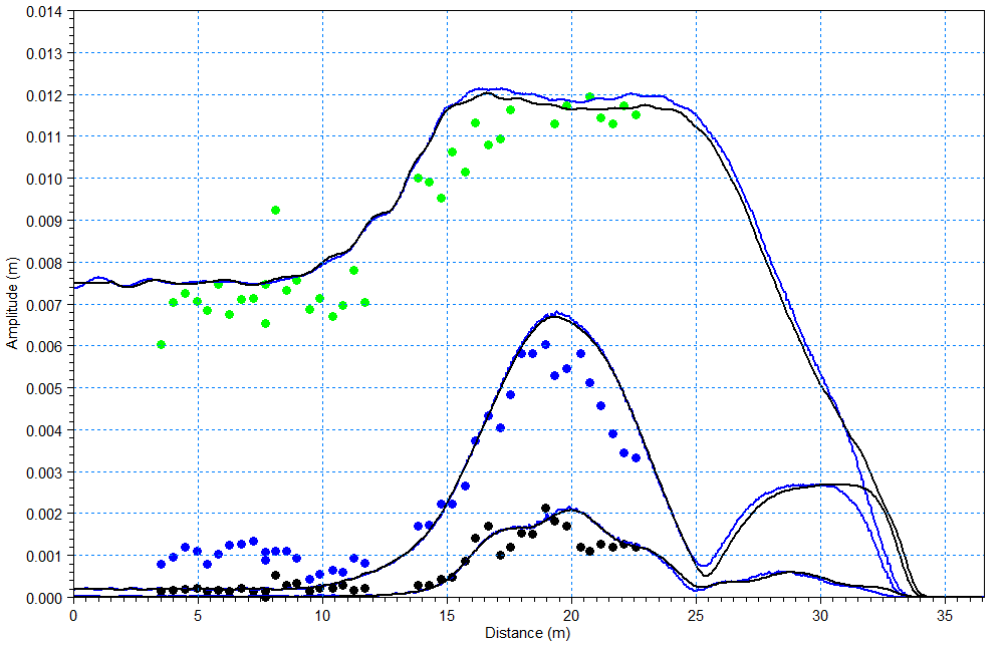

Figure 3.9 Wave amplitude for the first, second and third harmonic along the centreline. (T = 2s and H = 0.015m). Black line: Structured mesh; Blue line: unstructured mesh.; Green, blue and black circles: Experimental data by Whalin (1971) for first, second and third harmonics.

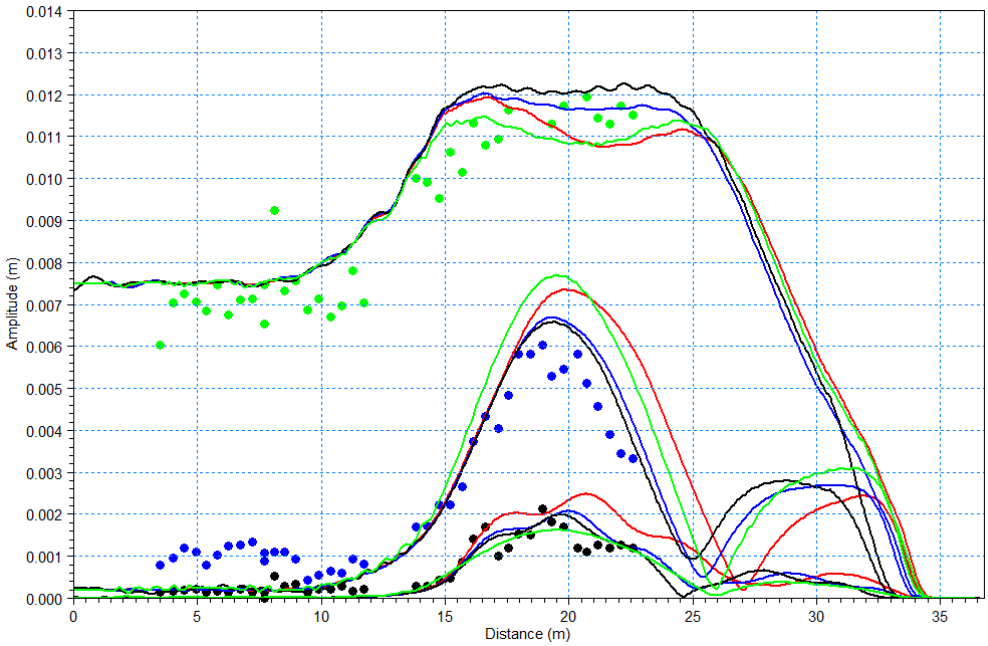

Figure 3.10 Wave amplitude for the first, second and third harmonic along the centreline. (T = 2s and H = 0.015m). Structured mesh. Red line: grid spacing 0.2032m; Green line: grid spacing 0.1016m; Blue line: grid spacing 0.0508m; Black line: grid spacing 0.0254m; Green, blue and black circles: Experimental data by Whalin (1971) for first, second and third harmonics.

3.3 Wave Runup on a Gently Sloping Beach

3.3.1 Description

The test case is widely used in connection with calculation of short waves using higher order models, such as Boussinesq models. See e.g. Madsen et al. (1997). The case shows the ability of the MIKE 21 Wave Model FM to handle flooding and drying on a sloping bottom.

The computational domain is 15m long with a constant slope of 1:25. The west (deepest end) boundary has the depth of 0.5m at mean water level. A wave with amplitude of 0.003m and a period of 10s is applied to the west boundary.

An analytical solution exists for the case. See e.g. Carrier and Greenspan (1958).

3.3.2 Setup

Both a structured and an unstructured mesh are used. The meshes cover a domain of 5m by 15m. The structured mesh consists of 7500 uniform quadrilateral elements with an edge length of 0.1m. The unstructured mesh consists of 10405 triangular elements. The elements vary in size, the largest being approximately 0.04m2 in the deepest end and the smallest being approximately 0.003m2 in the shallow end. The grid is seen in Figure 3.11. The incoming waves are specified using a relaxation zone: Line from (x,y)=(0.5m, 5.0m) to (x,y)=(0.5m, 0.0m) and the width of the ramp-up zone is 0.4m. The waves are generated using 1st order Stokes theory.

Simulations have been performed using the HLLC solver with a Riemann factor of 0.25. No eddy viscosity has been applied.

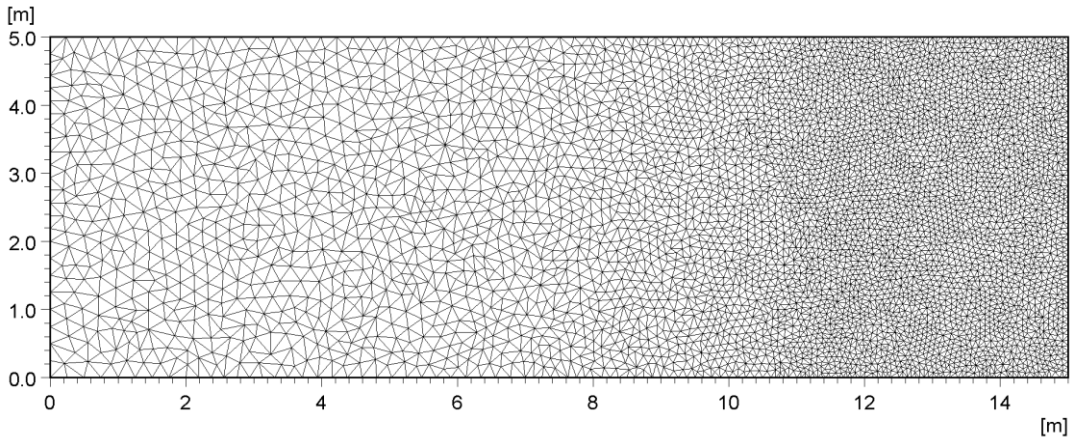

Figure 3.11 Computational mesh used in the wave on a sloping beach case.

3.3.3 Results

Figure 3.13The results are shown in Figure 3.12 and Figure 3.13. As seen, the results using both the structured and the unstructured mesh are in very good agreement with the analytical solution.

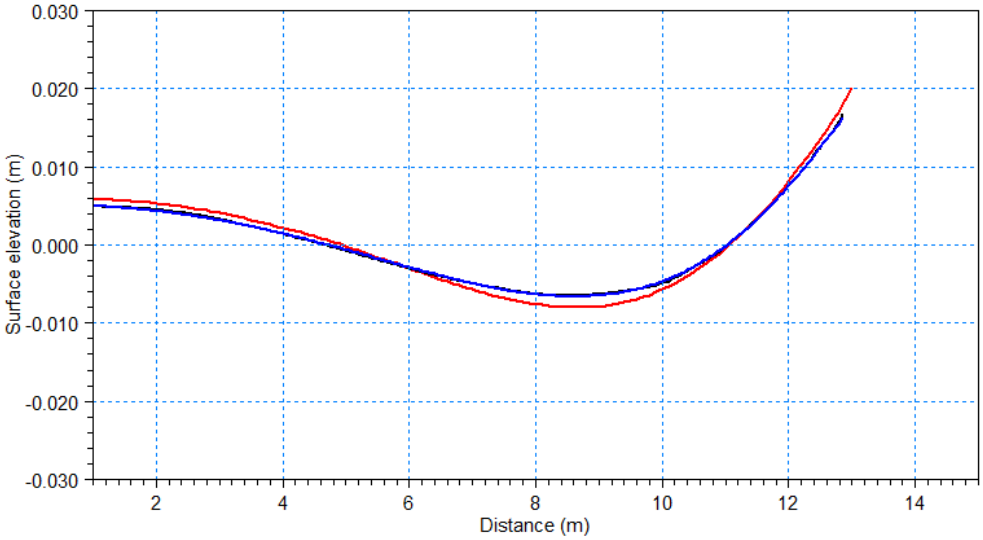

Figure 3.12 Cross-shore variation of surface elevation at the maximum elevation on the boundary. Black line: MIKE 21 Wave Model FM (structured mesh); Blue line: MIKE 21 Wave Model FM (unstructured mesh); Red line: Analytical solution.

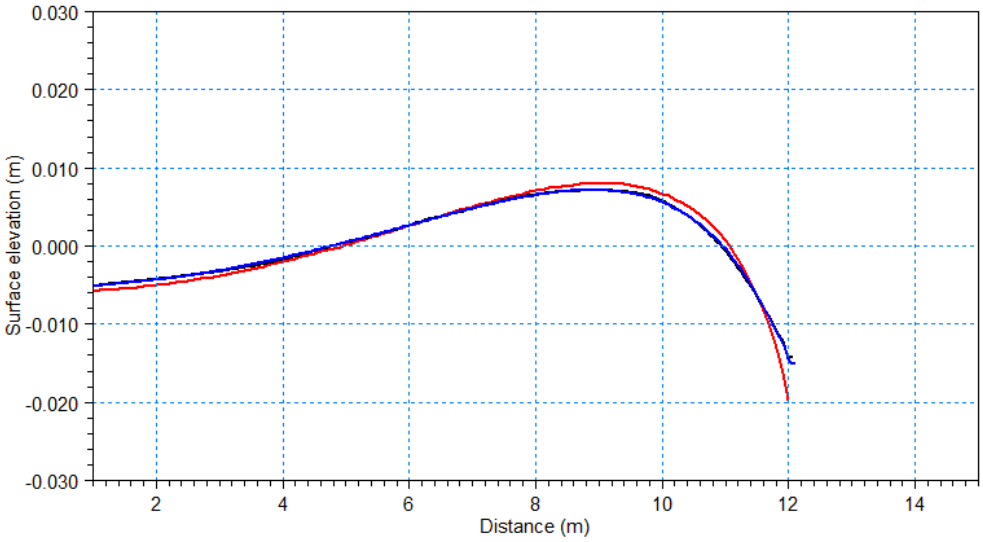

Figure 3.13 Cross-shore variation of surface elevation at the minimum elevation on the boundary. Black line: MIKE 21 Wave Model FM (structured mesh); Blue line: MIKE 21 Wave Model FM (unstructured mesh); Red line: Analytical solution.

3.4 Shoaling and Breaking of Regular Waves on a Gently Sloping Beach

3.4.1 Description

Ting and Kirby (1994) presented measurements for both spilling breakers and plunging breakers on a plane sloping beach with a slope of 1/35 starting at a depth of 0.40m. The numerical setup is shown in Figure 3.14. As input, they generated for the spilling breakers case regular waves with a period of 2.0s and a wave height of 0.125m and for the plunging breaker case regular waves with a period of 5.0s and a wave height of 0.128m.

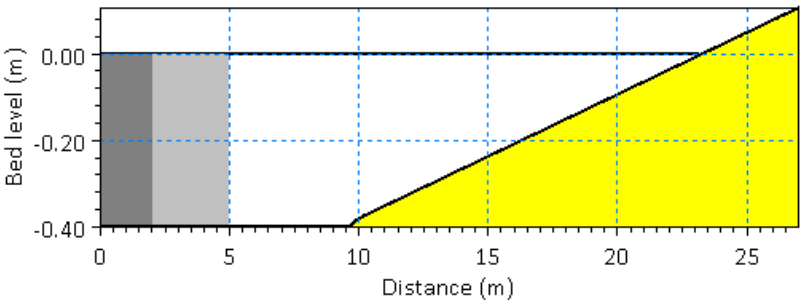

Figure 3.14 Sketch illustrating numerical setup.

3.4.2 Setup

This test case is a one-dimensional flow problem. Hence, a one-element wide channel is used in the simulation. The mesh consists of quadrilateral elements with an edge length of 0.02m are. The incoming waves are specified using a relaxation zone: Line from (x,y)=(5.0m, 0.02m) to (x,y)=(5.0m, 0.0m) and the width of the ramp-up zone is 3.0m. The waves are generated using the Boussinesq 3rd order wave theory for the spilling breakers and Cnoidal wave theory for the plunging breaker case.

Simulations have been performed using the HLLC solver with a Riemann factor of 1.00. Neither eddy viscosity nor bed friction have been applied. For the spilling breaker case the default values for the breaking parameters are used: a roller factor of 1.5, an initial breaking angle of 20deg, a final breaking angle of 10deg, a velocity factor of 1.3. and time scale for the roller development of T/5=0.4s. For the case with plunging breakers, the roller factor is increased to 2, the initial breaking angle is increased to 25deg and for the time scale for the roller development T/10=0.5s is used.

3.4.3 Results

The cross-shore variation of the wave crest elevation, wave trough elevation and mean water level are shown in Figure 3.15 and Figure 3.16. Here the results using MIKE 21 Wave Model FM are compared with the results using MIKE 3 Wave Model FM. It is seen that MIKE 21 Wave Model underestimate the nonlinear shoaling, especially for the spilling breakers case. The reason for this discrepancy is that the enhanced Boussinesq equations underestimate the transfer of energy to the superharmonics. However, MIKE 21 Wave Model gives a good prediction of the variation in the surf zone of the wave height and setup. Especially for the plunging breaker case a secondary peak in the elevation can be seen to evolve in the inner surf zone due to limitation in the breaker model. It can also be seen that the prediction of the nonlinear shoaling is significantly improved using MIKE 3 Wave model.

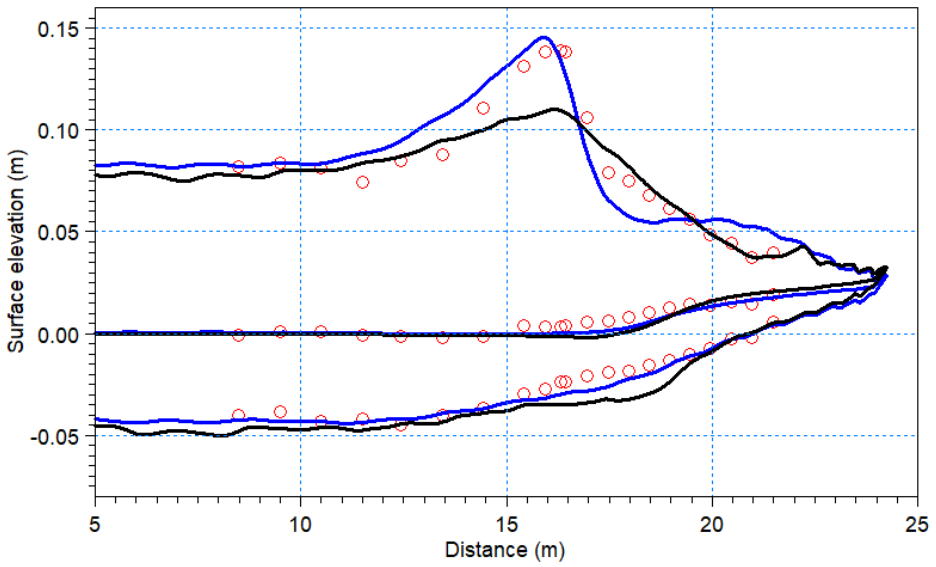

Figure 3.15 The cross-shore variation of the wave crest elevation, wave trough elevation and mean water level for the test of Ting and Kirby (1994) with spilling breakers (T=2s). Black line: MIKE 21 Wave Model FM, Blue line: MIKE 3 Wave Model FM; Red circles; experimental data.

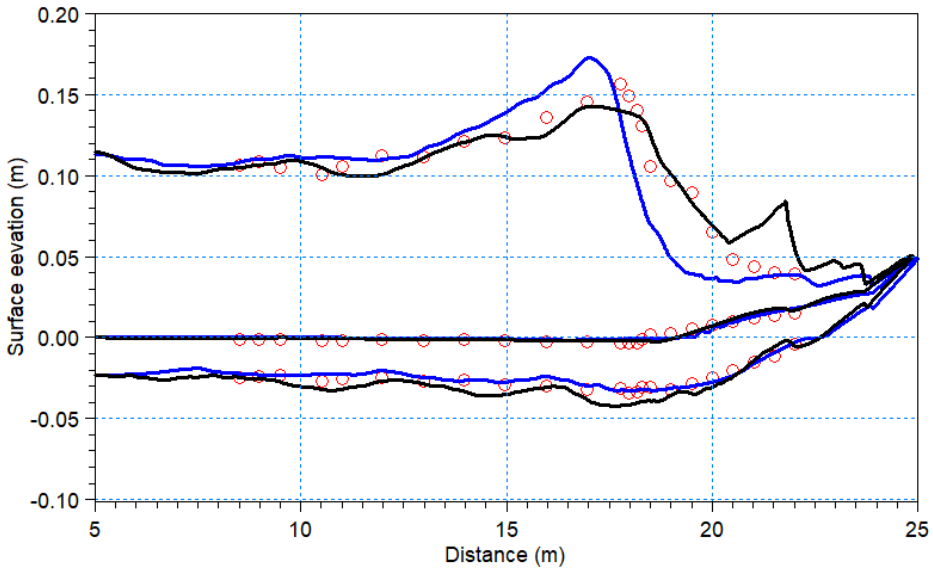

Figure 3.16 The cross-shore variation of the wave crest elevation, wave trough elevation and mean water level for the test of Ting and Kirby (1994) with plunging breakers (T=5s). Black line: MIKE 21 Wave Model FM, Blue line: MIKE 3 Wave Model FM; Red circles; experimental data.

3.5 Rip Channel

3.5.1 Description

Laboratory experiments for a case with wave propagation on a plane beach with a rip channel have been reported by Hamm (1992a,b). The wave basin is 30m x 30m and the bathymetry is a plane sloping beach of 1:30 with a rip channel excavated along the centreline. The depth variation is given by

$$h(x,y)=\begin{cases}0.5 & x\le 7\\ -0.1+\dfrac{25-x}{30}\left[1+3\exp\left(-\dfrac{25-x}{3}\right)\cos^{10}\left(\dfrac{\pi(15-y)}{30}\right)\right] & 7<x<25\\ -0.1+\dfrac{25-x}{30} & x\le 25\end{cases}$$

Hamm considered a number of different incident wave conditions. Here the case with unidirectional, regular, incident waves with a period of 1.25s and a wave height of 0.07m is considered.

3.5.2 Setup

Only half of the physical wave tank is covered in the computations, and reflective boundary conditions are applied at the line of symmetry. Simulations are performed using both a structured quadrilateral mesh with 80000 elements and an unstructured triangular mesh also with 80000 elements. The incoming waves are specified using a relaxation zone: Line from (x,y)=(2.0m, 15.0m) to (x,y)=(2.0m, 0.0m) and the width of the ramp-up zone is 1.0m. The waves are generated using 3rd order Bousinnesq theory. The simulation period is 300s corresponding to 240 wave periods. Simulations are also performed using the full domain, where the mesh is created by symmetry of the half domain across the centreline. Hence, the quadrilateral mesh and triangular mesh for the full domain consist of 160000 elements.

Simulations are performed using the HLLC solver with a Riemann factor of 0.25. No eddy viscosity is used. For the full domain a simulation is also performed using the Smagorinsky formulation for the eddy viscosity with a constant value of 0.2. Bed friction is applied with a Manning number of 40 m**1/3/s. Explicit breaking is applied using the default values for the breaking parameters.

3.5.3 Results

Due to the difference in the wave set-up along the rip channel, and at the plane beach away from the rip channel there is an alongshore gradient in the mean water surface elevation. This gradient will force a current towards the centreline. The flow from both sides will join to form a rip current and two symmetrical circulation cells will be created. A steady-state current field will be reached when the forcing due to the gradient in the mean surface elevation is balanced out by the bed friction.

Figure 3.17 shows the cross-shore variation of the wave height at some distance from the rip channel where the beach is a plane slope. A plot along the excavated beach at the centreline is shown in Figure 3.18. The measurements of Hamm are included and the agreement is quite good. A vector plot of the time-averaged velocity field is shown in Figure 3.19 and Figure 3.20 for the mesh with quadrilateral elements and triangular elements. A subdomain is shown in order to focus on the circulation cell. The velocity is computed as the time-average of the depth-averaged velocity. The velocity vectors are shown in a structured grid. A pronounced rip current is seen along the centreline of the bathymetry, i.e. at the top of the figure. A formation of small eddies along the plane beach can also be identified. However, more detailed data are needed to show if similar eddies are actually present in the physical experiment. The cross-shore variation of the velocity along the centreline is shown in Figure 3.21. The maximum current speed is 0.22m/s for the simulation using quadrilateral elements and 0.20m/s for the simulation using triangular elements. In the physical experiments, an instability of the rip current could be seen and a maximum of 0.25m/s for the mean return current near the bottom was measured.

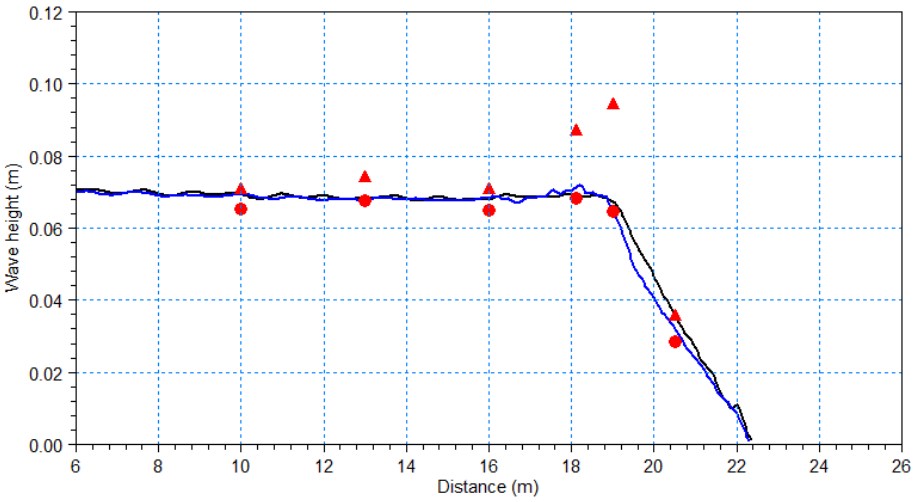

Figure 3.17 Comparison between the computed and measured cross-shore variation of the wave height. Black line: MIKE 21 Wave Model FM (structured mesh); Blue line: MIKE 21 Wave Model FM (unstructured mesh). ▲ Experimental data by Hamm (1992b) - Significant wave height, $H_{1/3}$: ● Experimental data by Hamm (1992b) - Variance-based wave height $H_o/\sqrt{2}$.

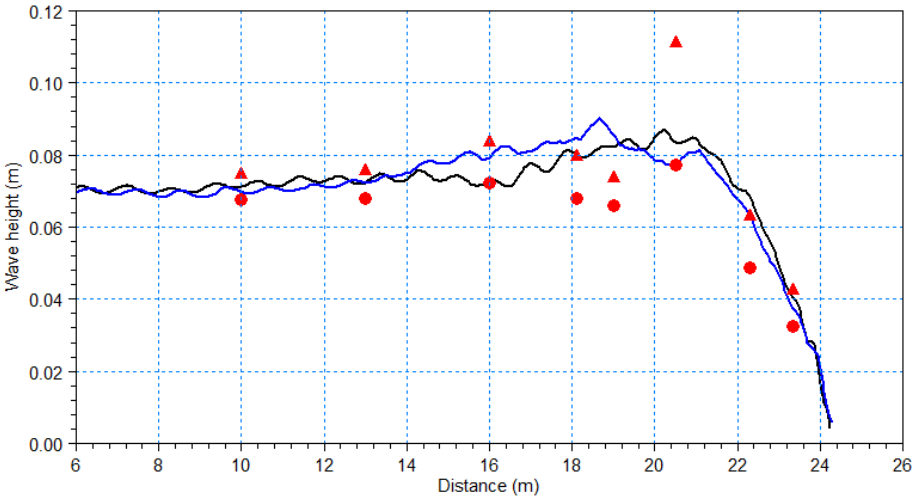

Figure 3.18 Comparison between the computed and measured cross-shore variation of the wave height. Black line: MIKE 21 Wave Model FM (structured mesh); Blue line: MIKE 21 Wave Model FM (unstructured mesh). ▲ Experimental data by Hamm (1992b) - Significant wave height, $H_{1/3}$; ● Experimental data by Hamm (1992b) - Variance-based wave height $H_\sigma/\sqrt{2}$.

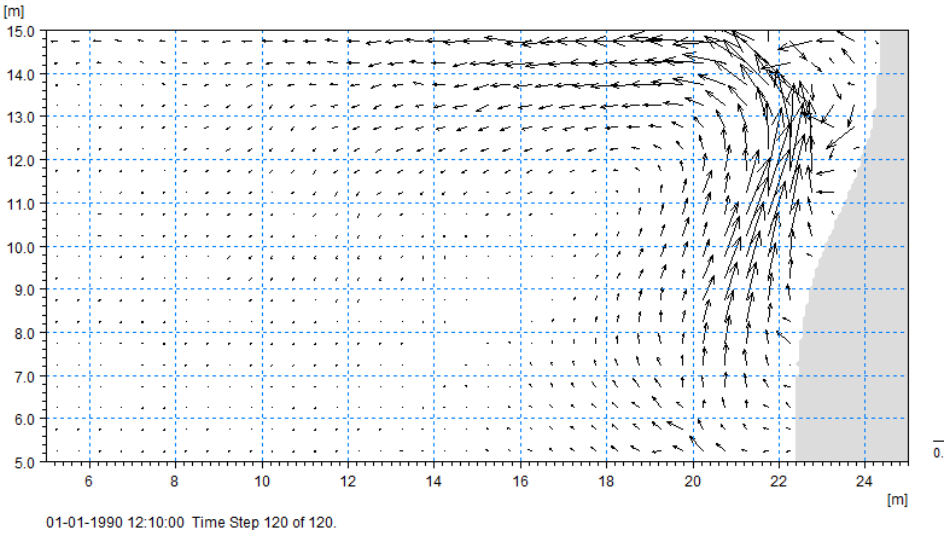

Figure 3.19 Mean velocity focusing on the circulation cell. Mesh with quadrilateral elements.

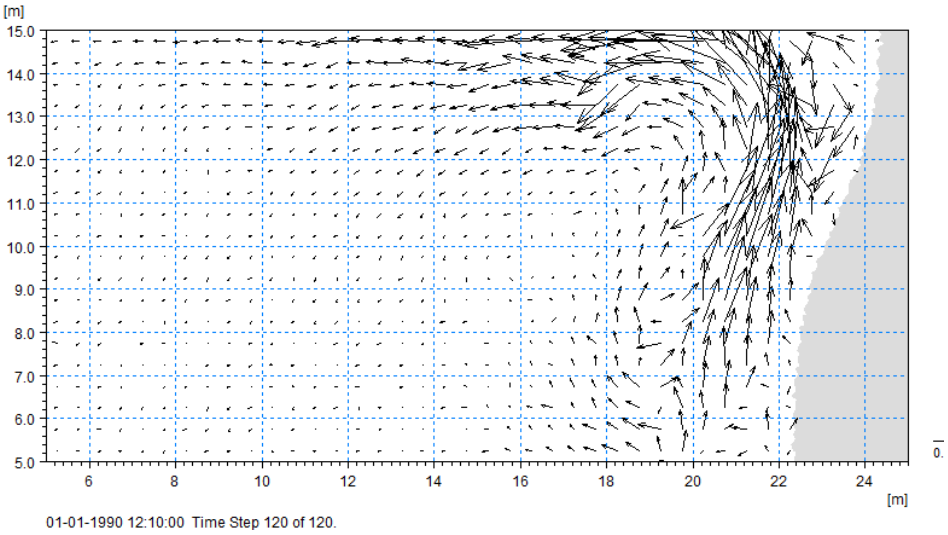

Figure 3.20 Mean velocity focusing on the circulation cell. Mesh with triangular elements.

Simulations have also been performed using the full domain. For a simulation without eddy viscosity the rip current becomes unstable. This is shown in Figure 3.22 showing a time series of the mean current speed at three positions along the centreline. In Figure 3.23 is shown the mean current velocity field in a subdomain. If eddy viscosity is included using the Smagorinsky formulation with the constant value of 0.2 a stable rip current is obtained as shown in Figure 3.24. The cross-shore variation of the velocity along the centreline for the case with eddy viscosity is also shown in

Figure 3.21. Using the triangular mesh and an eddy viscosity with the Smagorinsky constant of 0.2 a stable rip current is also obtained, but some asymmetry can be seen in the flow field.

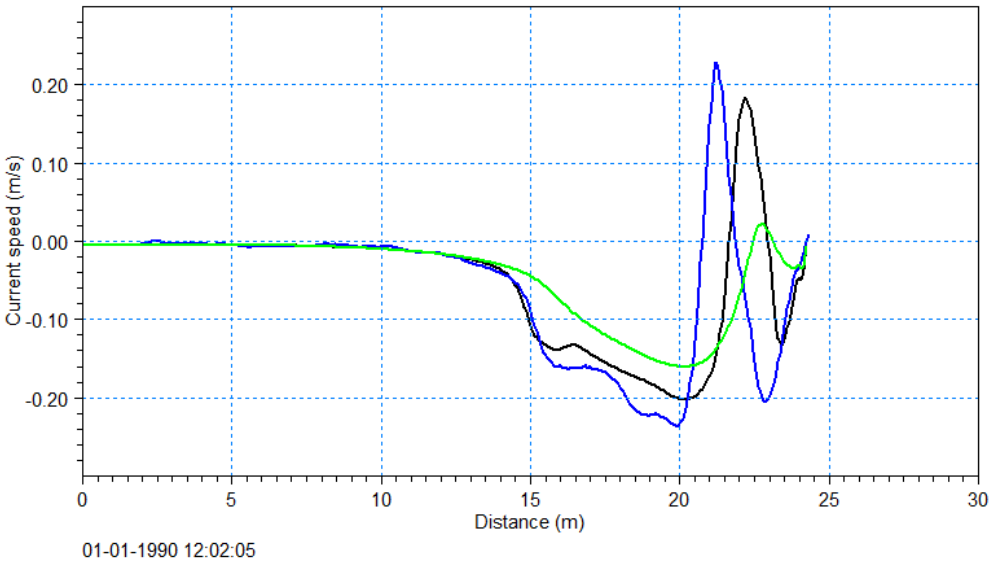

Figure 3.21 Rip current along the centreline. Black line: Half domain with structured quadrilateral mesh; Blue line: Half domain with unstructured triangular mesh; Green line: Full domain with structured quadrilateral mesh and simulation using eddy viscosity (Smagorinsky formulation with constant value of 0.2)

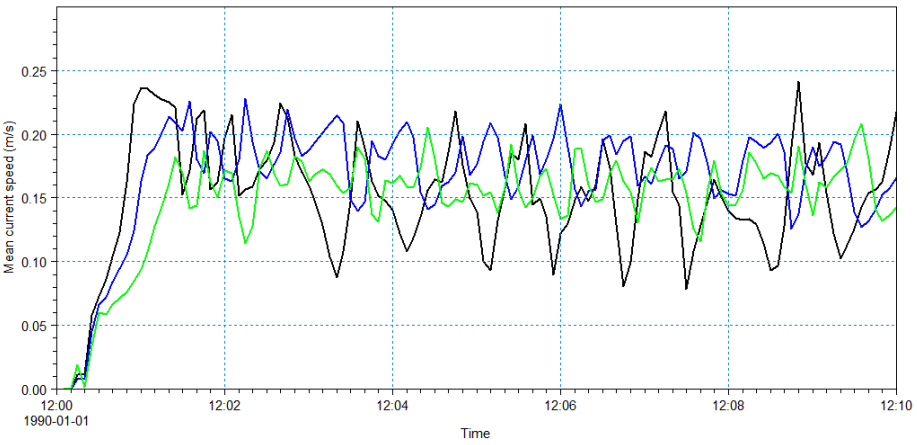

Figure 3.22 Time series of mean velocity at three positions along the centreline (19,15), (20,15) and (21,15). Full domain with quadrilateral elements. Simulation without eddy viscosity. Green line: (x, y)=(19m,15m); Blue line: (x, y) = (20m, 15m); Black line: (x, y) = (21m, 15m).

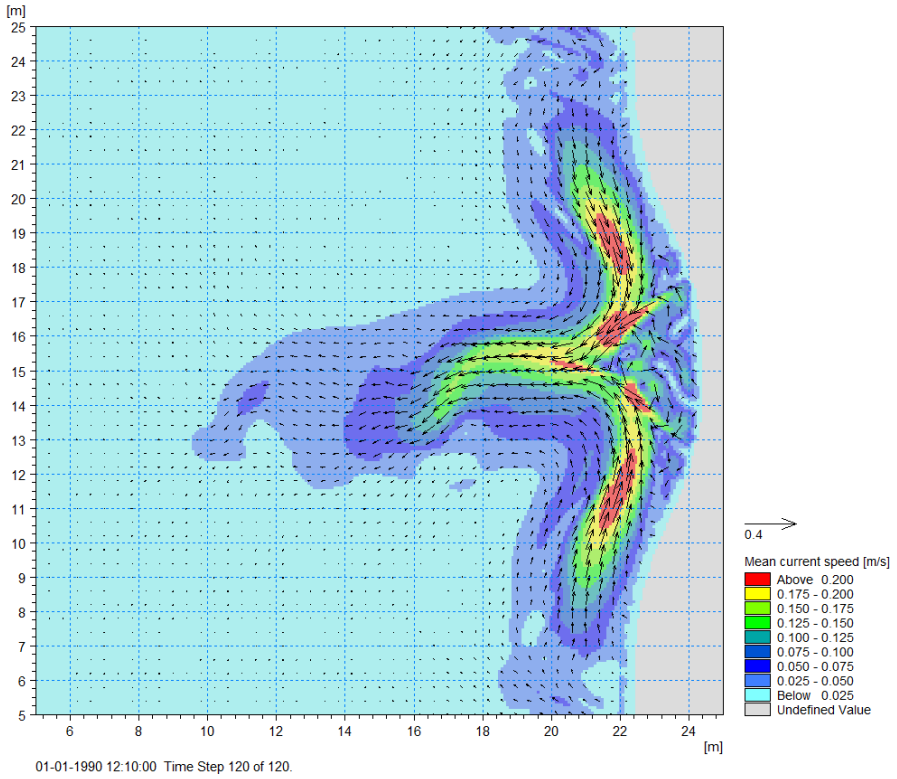

Figure 3.23 Mean velocity focusing on the circulation cell. Full domain with quadrilateral elements. Simulation without eddy viscosity.

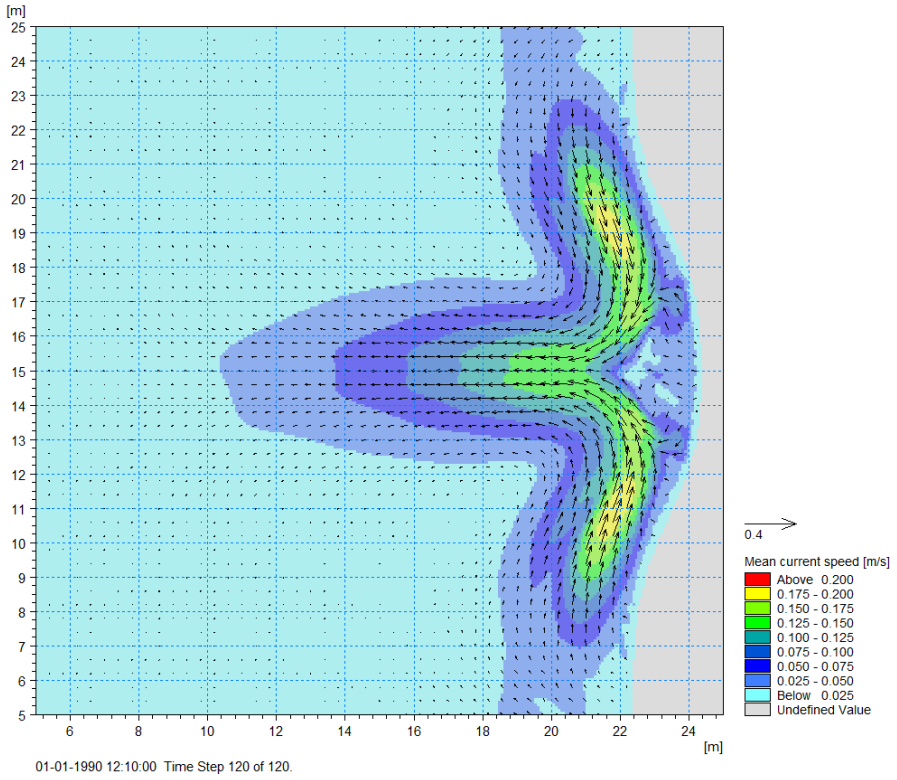

Figure 3.24 Mean velocity focusing on the circulation cell. Full domain with quadrilateral elements. Simulation using eddy viscosity (Smagorinsky formulation with constant value of 0.2).

3.6 Porous Dam-break

3.6.1 Description

This test considers a dam-break through a porous structure. The model results are compared to the laboratory results given in Liu et al. (1999). The laboratory experiment was conducted in a wave tank that is 89.2cm long, 44cm wide and 58cm high. The porous structure is 29cm long, 44cm wide and 37cm high, and it is placed at x = 30.0-59.0cm, see Figure 3.25. A gate is placed 2cm to the left of the porous structure. On the left side of the gate the initial water depth, h, is about 25cm and on the right side of the gate it is 2.5cm. The porous structure consists of crushed rocks with an average diameter of 1.59cm, leading to a final porosity of 0.49. The experiment was started by removing the gate and hereby allowing the water to flow through the porous structure. The gate was removed manually within about 0.1s.

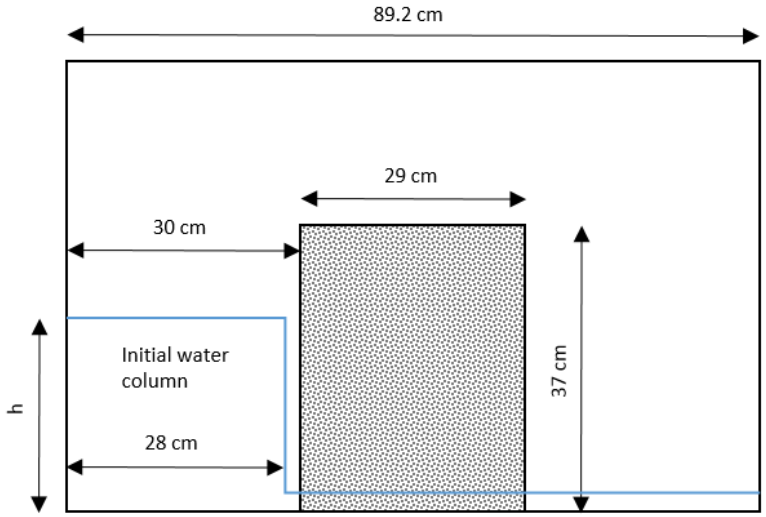

Figure 3.25 Initial porous Dam-Break setup.

3.6.2 Setup

For the numerical experiment, a structured mesh consisting of 223 quadrangular 2D elements is used. The grid spacing in the flow direction is $\Delta x = 0.4$m, whereas Δy is the full width of the tank. The values of the linear and nonlinear friction parameters are set to $\alpha = 500$ and $\beta = 2$. The oscillating period is here set to 10s.

Simulations have been performed using the HLLC solver with a Riemann factor of 1.00. No eddy viscosity is used.

3.6.3 Results

The results of the numerical model are presented in Figure 3.26. For comparison, the laboratory results given in Liu et al. (1999) are plotted as red circles in the figure.

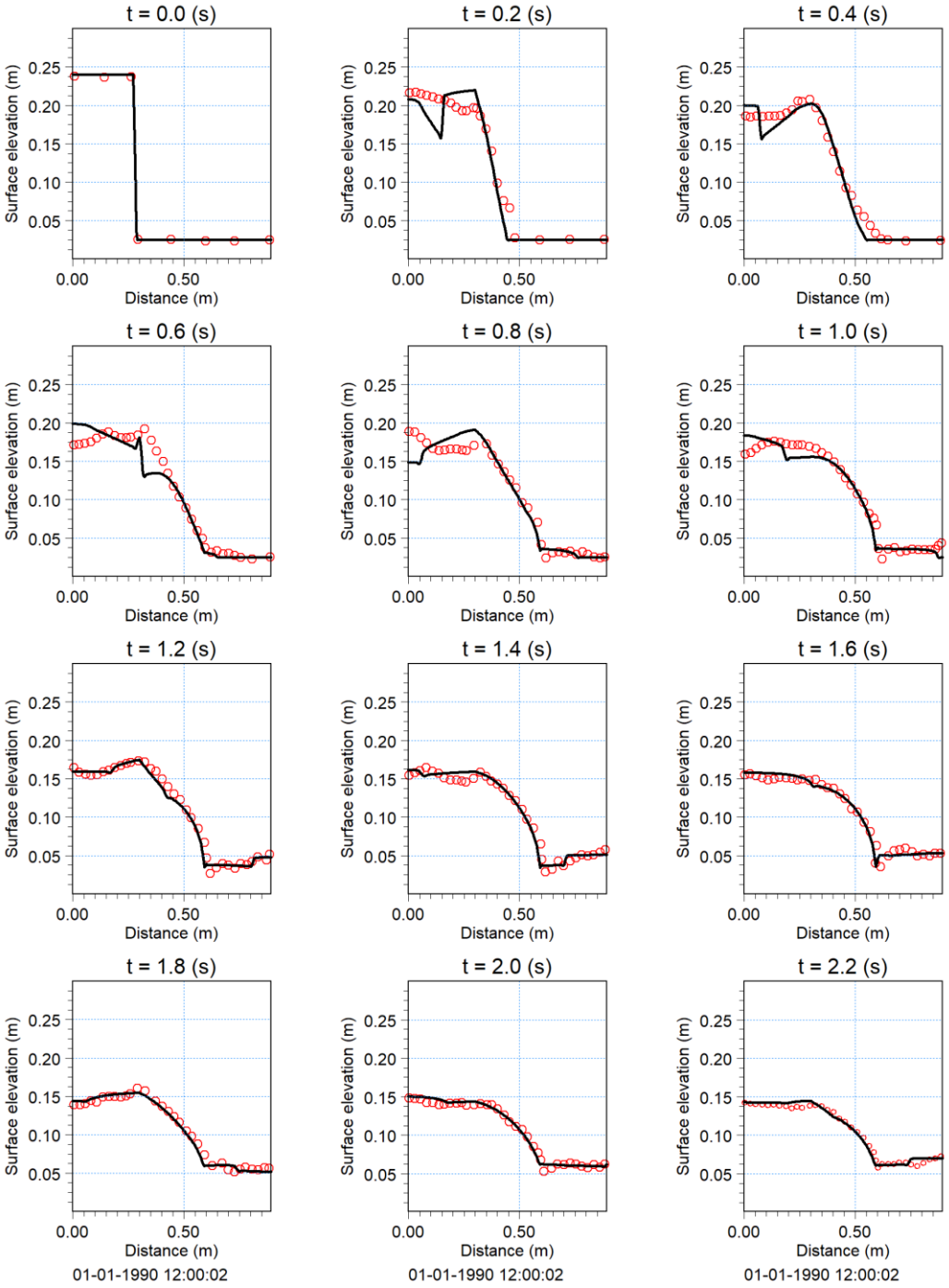

Figure 3.26 Comparison of the numerical computed surface elevation and the laboratory results given in Liu et al. (1999). Black line: Numerical results. Red circles: Laboratory results.

As illustrated in Figure 3.26, the numerical results agree reasonably with the measured lab results. However, it is seen that the reflection from the front of the porous structure seem to be too high.

3.7 Regular Waves Interacting with Vertical Porous Breakwater

3.7.1 Description

This test is validated against the experimental results presented in Lara et al. (2012). The test is conducted in a rectangular flume, which is 22m long, 0.585m wide and 0.78m high. A wave maker is positioned at the beginning of the flume, such that from the mean position of the wave maker to the end of the flume there is 20.595m. The wave maker has a stroke of ±0.45m. A porous structure being 0.24m long, 0.24m wide and 0.7m high is placed against the one side of the flume, such that the centre of the structure is located 11.519m from the mean position of the wave maker. Between the porous structure and the wall an impermeable block of plexiglass is placed. This block has a thickness of 0.06 m. See Figure 3.27 for an illustration of the experimental arrangement. The porous structure consists of crushed stones with a mean diameter of 0.0083m, leading to a final porosity of 0.48.

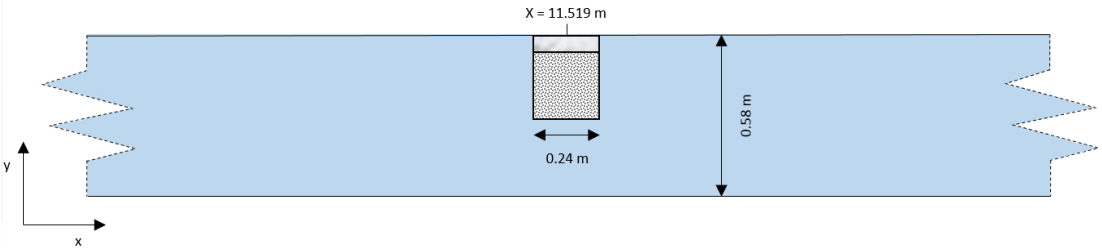

Figure 3.27 Subset of the experimental arrangement in the area around the porous structure.

The flume is equipped with a number of wave gauges, which are located as indicated in Table 3.1 and Figure 3.28.

Wave Gauge	x-coordinate (m)	y-coordinate (m)
W1	10.299	0.1
W2	10.299	0.485
W3	11.299	0.1
W4	11.299	0.385
W5	11.499	0.185
W6	11.739	0.1
W7	11.739	0.385
W8	12.039	0.1
W9	12.039	0.485
W10	12.439	0.285
W11	12.839	0.1
W12	12.839	0.485

Table 3.1 Wave gauge locations.

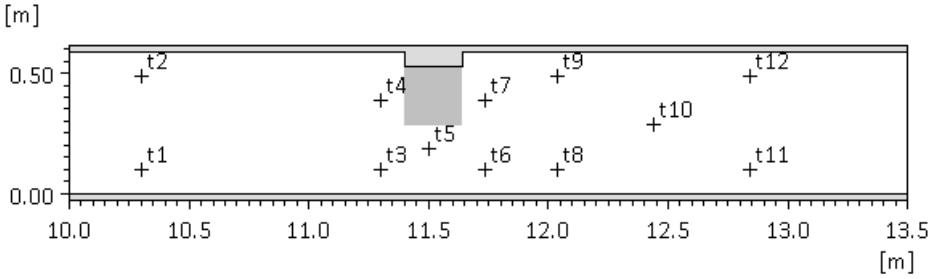

Figure 3.28 Wave gauge locations.

The experiment is run using regular waves with a period of 2s and a height of 0.06m. The mean water depth is 0.25m.

3.7.2 Setup

The numerical experiment uses quadrangular elements with a grid spacing in the range Δx = [0.02m, 0.04m] and Δy = 0.015m, resulting in a 2D mesh with 23040 elements. The grid is finest in the area around the porous structure, since this is the area of interest. A subset of the mesh is seen in Figure 3.29, which shows the mesh in the area around the structure.

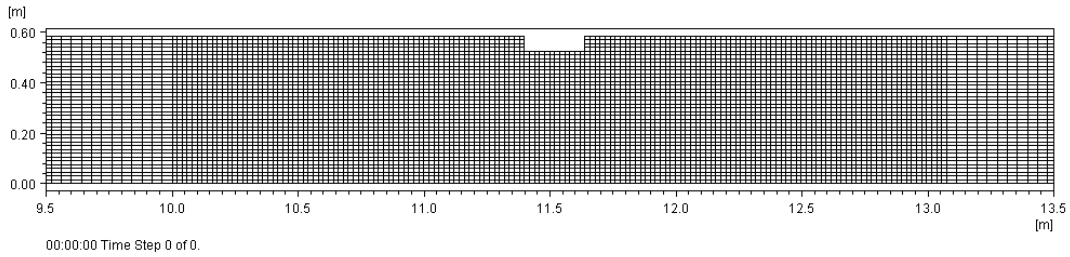

Figure 3.29 Subset of the computational mesh for the Vertical Porous Breakwater setup.

The waves are generated using a relaxation zone located at x = 1 m with a width of 0.8 m and using the Boussinesq 3rd order wave theory. The values of the linear and nonlinear friction parameters are set to α = 500 and β = 2.

Simulations have been performed using the HLLC solver with a Riemann factor of 1.00. No eddy viscosity is used.

3.7.3 Results

The numerical results for wave gauge 1-7 presented in Figure 3.30 are validated against the laboratory results given by Lara et al. (2012). The agreement is quite good both with respect to the phase and amplitude. Some discrepancies can be seen at the end of the time series, when the waves reflected from the end wall reach the area where the wave gauges are located. For comparison the results using MIKE 3 Wave Model FM is shown in Figure 3.30. The agreement between MIKE 21 Wave Model FM and MIKE 3 Wave Model FM is seen to be very good.

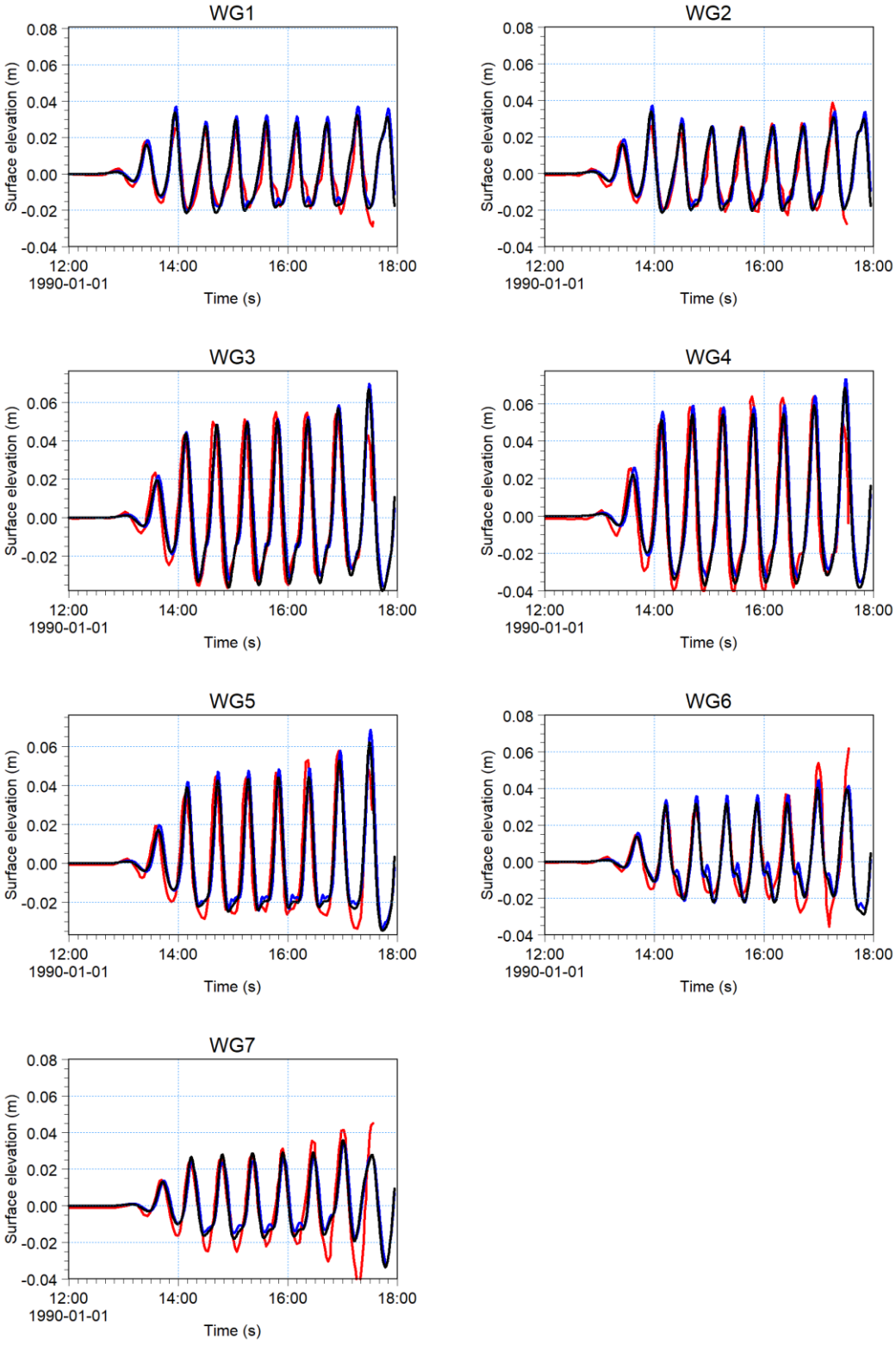

Figure 3.30 Computed and measured surface elevation at several locations. Black line: MIKE 21 Wave Model FM; Blue line MIKE 3 Wave Model FM; Red line: Experimental data.

3.8 Runup of Solitary Waves on a Conical Island

3.8.1 Description

This test aims to reproduce the experimental results for solitary wave runup on a circular conical island presented by Briggs et al. (1995). The test is conducted in a rectangular wave basin that is 25m long, 30m wide and 0.6m deep. Near the centre of the basin an island with the shape of a truncated circular cone is located. The cone has a diameter of 7.2m at the toe and 2.2m at the crest. The slope of the cone is 1/4 leading to a height of approximately 0.625m. A wave maker is located at one end of the basin. The coordinate system is chosen such that the centre of the island is located x = 12.96m from the wave maker and y = 13.8m from the side of the basin. The basin sides and rear are lined with absorbers to reduce reflections. The experiment is performed using two different water depths, d = 0.32m and 0.42, but only the first one is considered in this study.

Three different cases of wave heights relative to the depth, h/d, are considered for the solitary wave generated in the experiment:

- Case A: h_{target}/d = 0.05, $h_{measured}/d$ = 0.045
- Case B: h_{target}/d = 0.10, $h_{measured}/d$ = 0.096
- Case C: h_{target}/d = 0.20, $h_{measured}/d$ = 0.181

Note, that the relative target and measured wave hights differ slightly. Twenty-seven wave gauges for measuring surface elevation are located in the basin. In this study only the eight wave gauges listed in Table 3.2 are considered. The maximum vertical runup is measured at twenty locations around the island.

Wave Gauge	x-coordinate (m)	y-coordinate (m)
WG1	A: 5.76, B: 6.82, C: 7.56	16.05
WG2	A: 5.76, B: 6.82, C: 7.56	14.55
WG3	A: 5.76, B: 6.82, C: 7.56	13.05
WG4	A: 5.76, B: 6.82, C: 7.56	11.55
WG6	9.36	13.80
WG9	10.36	13.80
WG16	12.96	11.22
WG22	15.56	13.80

Table 3.2 Wave gauge locations in experiment. Note, WG 1-4 have different locations for each of the three test cases.

3.8.2 Setup

The numerical experiment considers a slightly larger domain that is 26m long and 30m wide, x = [-1;25] and y = [-15;15]. This is to give room for a 1m wide wave generation zone at x = [-1;0]. The domain is designed such that the conical island is located at (x,y) = (13,0). At the right end of the domain a 5m wide sponge layer is applied to reduce reflections.

A subset of the domain showing the island geometry and the wave gauge locations used in test case C is shown in Figure 3.31.

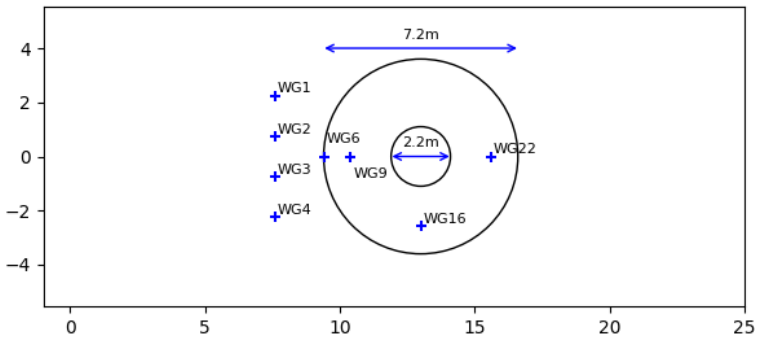

Figure 3.31 Subarea of domain showing island geometry and the wave gauge locations for test C.

Four different meshes are considered in the numerical experiment: There are three meshes with structured quadrilateral elements and a mesh with triangular elements. The mesh information are listed in Table 3.3.

Element type	Element area	No. of elements
Quadrangular	0.01m^2	78,000
Quadrangular	0.04m^2	19,500
Quadrangular	0.16m^2	4875
Triangular	Approx. 0.0035m^2 -0.08m^2	19,682

Table 3.3 Mesh information for the four different meshes used in the numerical experiment.

The triangular flexible mesh contains elements with varying areas. The finest resolution is in the area of the island, see Figure 3.32.

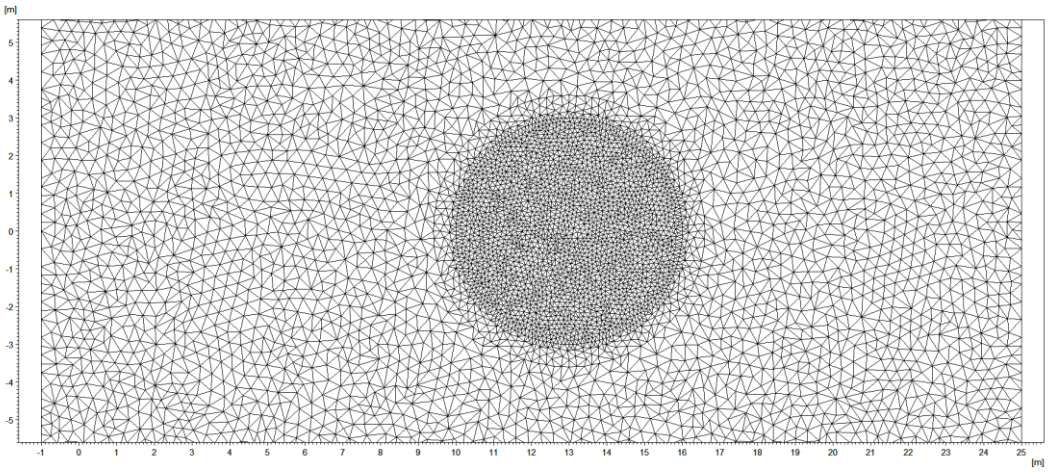

Figure 3.32 Subarea of triangular mesh showing finer resolution in the area of the island.

Like for the physical experiment, three different hight/depth ratios for the generated solitary wave are considered:

- Case A: *h/d* = 0.04
- Case B: *h/d* = 0.09
- Case C: *h/d* = 0.18.

Note, these ratios deviate slightly from the ratios reported by Briggs et al. (1995), since these ratios seem to have a better agreement with the measurements for the type of solitary waves considered in this study.

The simulations are performed using the HLLC Riemann solver with a Riemann factor of 1.0. No eddy viscosity is used. The flooding and drying parameters are set to 0.005m. No bed resistance is applied.

The wave gauges are located at the positions listed in Table 3.4, corresponding to the locations listed in Table 3.2, for the coordinate system considered in the numerical setup.

Wave Gauge	x-coordinate (m)	y-coordinate (m)
WG1	A: 5.80, B: 6.86, C: 7.60	2.25
WG2	A: 5.80, B: 6.86, C: 7.60	0.75
WG3	A: 5.80, B: 6.86, C: 7.60	-0.75
WG4	A: 5.80, B: 6.86, C: 7.60	-2.25
WG6	9.40	0.00
WG9	10.40	0.00
WG16	13.00	-2.58
WG22	15.60	0.00

Table 3.4 Wave gauge locations in numerical experiment. Note, WG 1-4 have different locations for each of the three test cases.

3.8.3 Results

In this section only the results for test case C are considered, since the solitary wave in this test case is the steepest of the waves in the three test cases, with a height to depth ratio of *h/d* = 0.18. The results of the numerical experiment are compared to the results presented by Briggs et al. (1995).

For test C the results at wave gauges 1-4 are very similar to each other. This is expected, since the bathymetry is flat between the wave generator and these wave gauges. Therefore, only the results for wave gauge 2 is presented, see Figure 3.33. As illustrated by this figure, all meshes, except the coarsest triangular mesh, produces similar results and are in relatively good agreement with the measurements. The deviations from the measurements are probably due to differences in the numerical and physical generation of the solitary wave. Similar conclusions are valid for test case A and test case B.

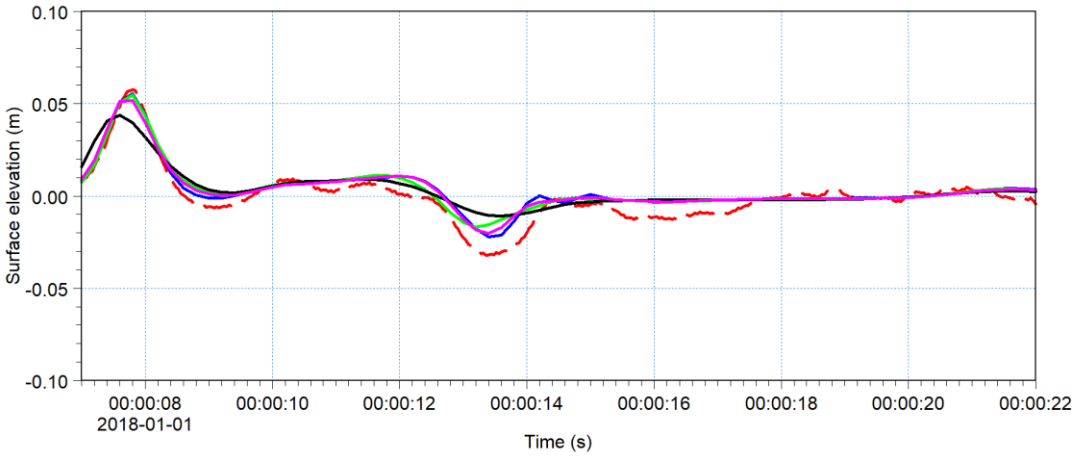

Figure 3.33 Surface elevation at wave gauge 2. Blue line: Quad 0.01m^2 mesh; Green line: Quad 0.04m^2 mesh; Black line: Quad 0.16m^2 mesh; Purple line: Tri mesh; Red dashed line: Measurements.

The results at wave gauges 6, 9, 16 and 22 clearly show the effect of mesh resolution, see Figure 3.34. For the quadrangular mesh with the finest resolution there is a relatively good agreement between the measured and calculated results. Again, some of the deviations in the results are explained with the difference in the numerical and physical generation of the solitary wave. Furthermore, differences between numerical and physical absorbers (sponge layers) could cause differences in reflections and diffraction.

As the mesh resolution for the quadrangular meshes gets more and more coarse, the agreement with the measurements gets worse, which is in line with theory. The quadrangular mesh with the coarsest resolution shows very poor agreement with the measurements.

The benefit of using a flexible mesh is also very well illustrated in Figure 3.34. The triangular mesh consists of approximately the same number of elements as the quadrangular mesh with element area 0.04m^2. However, the results using the triangular mesh agree much better with the measurements than using this quadrangular mesh, especially for wave gauge 22. In fact, the results using the triangular mesh is very close to the results using the finest quadrangular mesh, which consists of roughly four times as many elements.

The same conclusions regarding mesh resolution are reached when looking at the normalised maximum horizontal runup, see Figure 3.35. This figure illustrates that the finest quadrangular mesh and the flexible tridiagonal mesh are in good agreement with the measurements, whereas the coarser meshes show less good agreement.

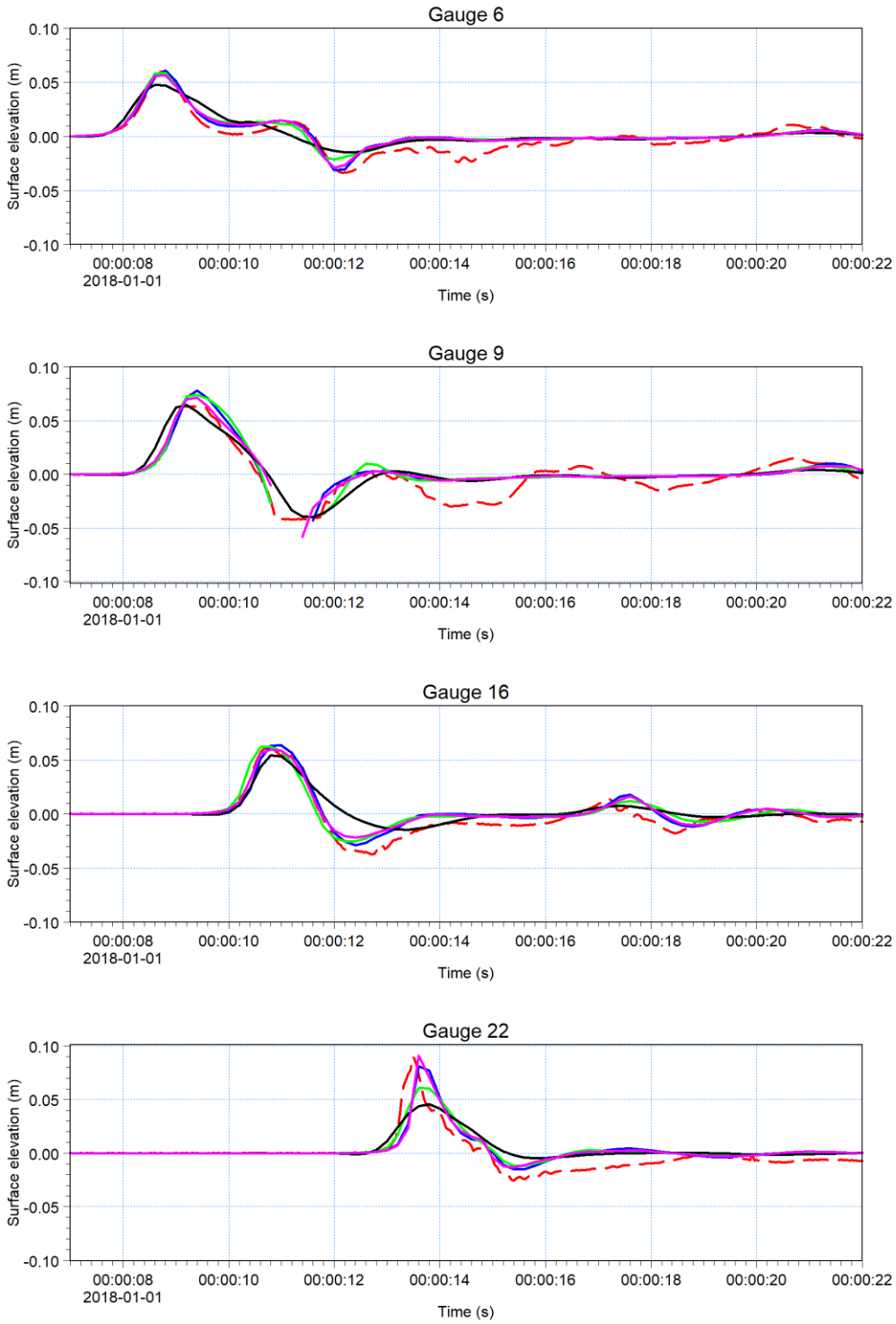

Figure 3.34 Surface elevation at wave gauges 6, 9, 16 and 22. Blue line: Quad 0.01m^2 mesh; Green line: Quad 0.04m^2 mesh; Black line: Quad 0.16m^2 mesh; Purple line: Tri mesh; Red dashed line: Measurements.

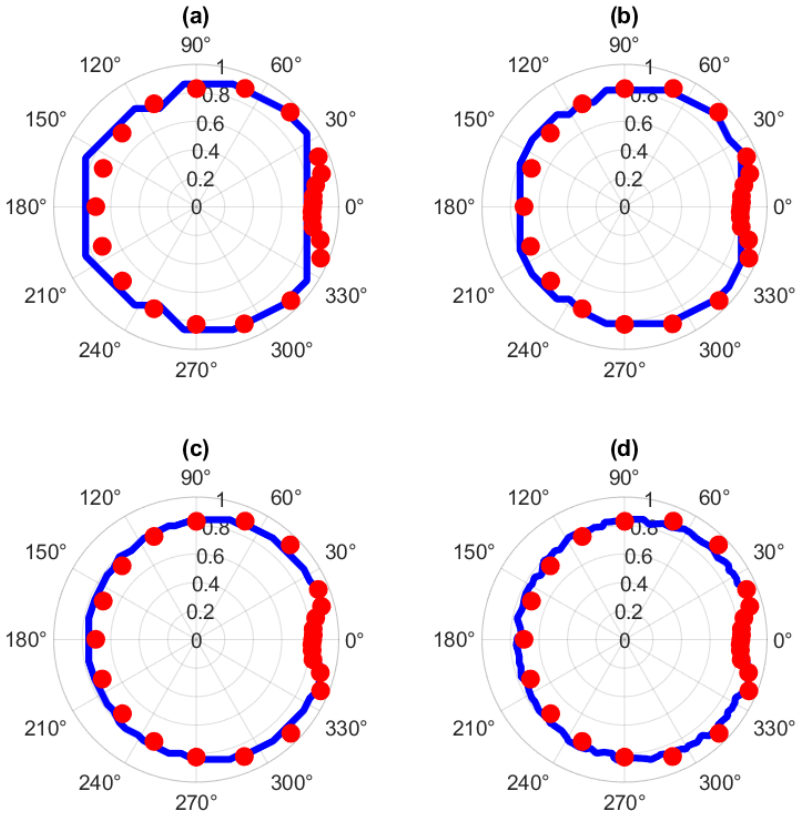

Figure 3.35 Normalised maximum horizontal runup for each of the four meshes. (a): Quad 0.16m^2 mesh; (b): Quad 0.04m^2 mesh, (c): Quad 0.01m^2 mesh, (d): Tri mesh.

4 References

/1/ Briggs, M.J., Synolakis, C.E., Harkins, G.S. and Green D.R., (1995): Laboratory experiments of tsunami runup on a circular island, *Pure Appl. Geophys.*, 144, pp 569-593

/2/ Carrier, G. F and Greenspan, H. P., (1958): Water Waves of Finite Amplitude on a Sloping Beach, *Journal of Fluid Mechanics vol 4*

/3/ Hamm, L., (1992a), Directional nearshore wave propagation over a rip channel: an experiment, *Pro. 23rd Int. Conf. Coastal Eng., Venice, Italy, 1992*, pp 226-239.

/4/ Hamm, L., (1992b), Random wave propagation in the nearshore zone: experiments in a directional wave basin, *Internal Report, MAST-G6M, SOGREAH*.

/5/ Lara, J. L., del Jesus, M. and Losada, I. J., (2012), Three-dimensional interaction of waves and porous coastal structures. Part II: Experimental validation, *Coastal Eng.*, **64**, 26-46.

/6/ Liu, P.L.-F., Lin, P., Chang, K.-A. and Sakakiyama, T., (1999), Numerical modeling of wave interaction with porous structures, J. Waterw. Port Coast. Ocean Eng., 125, 322-330

/7/ Madsen, P. A., Murray, R. and Sørensen, O. R., (1991), A new form of the Boussinesq equations with improved linear dispersion characteristics. Part 1, *Coastal Eng.*, **15**, 371-388.

/8/ Madsen, P. A. and Sørensen, O. R., (1992), A new form of the Boussinesq equations with improved linear dispersion characteristic. Part II. A slowly-varying bathymetry, *Coastal Eng.*, **18**, 183-204.

/9/ Madsen, P. A., Schäffer, H. A. and Sørensen, O. R., (1997), Surf zone dynamics simulated by a Boussinesq type model. Part 1: Model description and cross-shore motion of regular waves, *Coastal Eng.*, **32**, 255-287.

/10/ Madsen, P. A., Sørensen, O. R. and Schäffer, H. A. (1997), Surf zone dynamics simulated by a Boussinesq type model. Part 2: Surf beat and swash oscillations for wave groups and irregular waves, *Coastal Eng*., 32 (4), 289-319.

/11/ Madsen, P. A. and Schäffer, H. A. (1999), A review of Boussinesq-type equations for surface gravity waves. In 'Advances in Coastal and Ocean Engineering', P.L.-F. Liu (ed.) 5, World Scientific Publ., pp 1-95.

/12/ Luth, H.R., Klopman, G. and Kitau, N., (1994), "Project 13G: Kinematics of waves breaking partially on an offshore bar; LDV measurements for waves with and without a net onshore current", Delft Hydraulics Report H1573, March 1994, 40pp.

/13/ Ting, F.C.K. and Kirby, J.T., (1994), Observation of undertow and turbulence in a laboratory surf zone, *Coastal Eng.*, **24**, 51-80.

/14/ Whalin, R. W., (1971), The limit of applicability of linear wave refraction theory in convergence zone, Res. Rep. H-71-3, U.S. Army Corps of Engineers, Waterways Expt. Station, Vicksburg, MS.